# Higher-order exceptional points: A route for flat-top optical filters

Nitzan Habler and Jacob Scheuer*
*School of Electrical Engineering, Tel-Aviv University, Tel-Aviv, Israel 6997801*

(Received 22 September 2019; accepted 23 March 2020; published 22 April 2020)

We study theoretically the formation and properties of higher-order exceptional points (EPs) in optical parity-time symmetric systems (PTSSs) consisting of a finite number of coupled resonators. The analysis shows that only *specific* configurations of such PTSSs exhibit high-order EPs. We derive the conditions for the formation of higher-order EP in these PTSSs and discuss the properties of the eigenmodes. By taking advantage of the fundamental link between EPs and the formation of a white-light cavity, we utilize the conditions at which high-order EPs are formed for designing broadband, maximally flat, optical filters. By selecting the coupling coefficients between the resonators accordingly we show the bandwidth of such coupled cavity filters cannot only be enhanced substantially compared to other common design approaches, but also provide flat spectral response where these design approaches fail completely.

DOI: 10.1103/PhysRevA.101.043828

## I. INTRODUCTION

Exceptional points (EPs) are point singularities in the parameters space of a system at which at least two of its eigenvalues and eigenvectors coalesce [1]. Such points are often associated with non-Hermitian systems, which exchange energy with the environment. The interest in EPs has risen in the last decade, mainly in the context of the quantum mechanical concept of parity-time symmetry, as systems possessing such symmetry can exhibit real eigenvalues even if they are not Hermitian. More recently, optical parity-time symmetric systems (PTSSs) have been gaining more and more interest due to their significant impact and potential for various applications, including optical sensing [2,3], switching [4], lasing [5–7] and more. Such systems require both gain and loss of equal magnitude and can exhibit both real and complex eigenvalues (frequencies or wave numbers). One of the interesting properties of PTSSs is that their eigenvalues (or at least some of them) can coalesce into a single value when the system parameters are set properly. Optical PTSSs have been studied and demonstrated using several different physical platforms, where the most commonly ones are coupled microresonators and coupled waveguides. Nevertheless, regardless the platform, most of the studies where focused on infinites periodic arrays [8–10] or on finite structures comprising two coupled elements [1,11–16], where only a handful of studies have been carried out for larger, finite, systems [17–21].

Recently, it was shown that EPs in PTSSs correspond to the formation of a unique scenario known as the white-light cavity (WLC) [22]. A WLC is a unique type of resonator that is designed to resonate over a broad, continuous range of frequencies, as shown and demonstrated by Wicht [23] and later on by Shahriar's group [24]. This is accomplished by introducing an intracavity element with negative group velocity ($n_g < 0$), designed to provide a phase shift with a slope that is opposite in sign and equal in magnitude to that accumulated by light propagation through the "conventional" part of the structure [23,25,26]. This phase element compensates for the regular phase accumulation in the structure and satisfies the resonance phase condition over a band of frequencies. Several solutions for realizing such a phase compensator have been proposed, including absorptive vapor cells [27] and lossy resonators [28]. The simplest example of the latter case is a conventional cavity [the left cavity, denoted as the "main" cavity and marked in blue in Fig. 1(b)], which is coupled to a lossy cavity [the right cavity, marked in black in Fig. 1(b)] constituting the phase element. The coupling coefficient $\kappa$ between the cavities can be chosen such that the round-trip phase of the main (blue) cavity is compensated by the phase shift induced by the black one over a range of frequencies. Consequently, the coupled cavity system resonates on a continuous frequency range. The structure depicted in Fig. 1 constitutes a WLC with a certain level of round-trip loss. However, by introducing the correct level of gain (equal to the loss in the black cavity) into the "main" cavity in this arrangement immediately leads to the formation of a PTSS which, as shown in Ref. [28], is at its EP.

The equivalence between the conditions for the formation of a WLC and those for the formation of an EP in the structure depicted in Fig. 1 is indicative of the intimate relations between WLCs and EPs. In particular, the properties of PTSSs at their EPs are similar to those of WLCs and, therefore, allow for transferring intuition and applications between the two.

The formation of WLC has been shown to be closely related to broadband, maximally flat filters [22]. A conventional optical filter, consisting of a single resonator, exhibits a Lorentzian transmission function that is maximal at its resonance frequencies [29]. Although such a spectral response may be useful for narrow linewidth filtering, for other applications, such as telecommunications, different transmission properties are desired. More specifically, a maximally flat filter (MFF or Butterworth filter) is a filter that is designed to have a flat frequency response across its passband. The

*kobys@eng.tau.ac.il

 

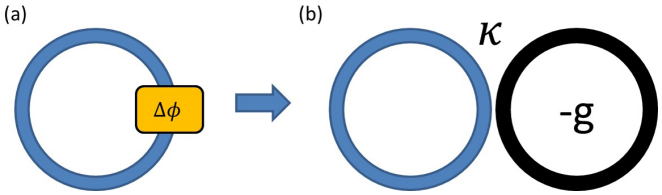


FIG. 1. (a) A general schematic of a WLC comprising a cavity and a phase element; (b) An example of an implementation of such phase compensator using a lossy resonator coupled to the "main" cavity.

flatness results in minimal signal distortions, as no ripple exists in the filter transfer function. It is well-known that an MFF can be realized by properly coupling several cavities having identical resonance frequency. Nevertheless, the optimization of the coupling coefficients is highly important as nonoptimal design may lead to a narrowband Lorentzian response or nonflat transmission profile [30–32] (see also Fig. 15 below).

A useful strategy for obtaining the optimal set of coupling coefficients was presented in Ref. [22]. Let us consider for example an optical filter comprising a single cavity and two I/O waveguides in as add-drop configuration [see Fig. 2(a)]. Maximal transmission (unity in the loss-less case) is obtained at the resonance frequencies and if the cavity is critically coupled. As the cavity resonates only at a discrete set of frequencies, maximal transmission is obtained only at these specific frequencies, thus leading to a nonflat transmission function. However, if the cavity can be made to resonate over a continuous range of frequencies, the corresponding frequency response of that filter would be maximal and flat over this range. The obvious way to extend the cavity resonance is to convert it into a WLC by introducing a phase compensation component $\Delta\phi$ as depicted in Fig. 2(a). As noted above, such phase component can be realized by an (additional) undercoupled cavity, leading to the double cavity filter structure depicted in Fig. 2(b). The value of the coupling coefficient $\kappa_2$ is determined by the WLC condition [22], while the equal coupling level to I/O waveguides, $\kappa_1$, guarantees that the WLC is critically coupled. The result is a MFF consisting of two coupled cavities.

It should be noted that other approaches for obtaining the coupling coefficients required for MFF have been

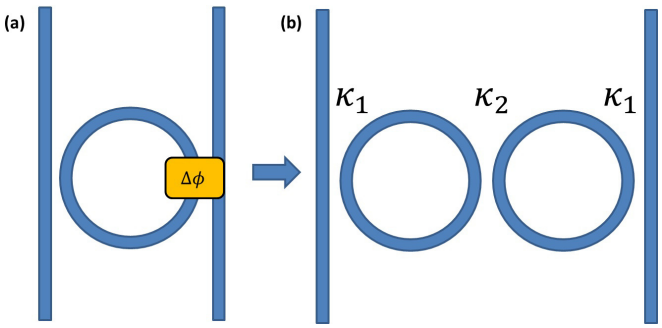


FIG. 2. (a) A general optical filter comprising a cavity and a phase element. (b) An example of phase compensation implementation using an additional cavity.

presented [30], using conventional filter design theory [33]. However, these approaches are valid only in the high loaded $Q$-factor approximation, which is not necessarily valid for ultra-broadband filters. The WLC approach for optical filter design has proven itself better than the approximate methods, leading to filters that exhibit flatter and broader frequency response [22]. Nevertheless the direct WLC based design approach is useful for designing filters comprising two or three cascaded cavities, and it is not obvious how it can be extended to higher-order filters.

In this paper, we utilize the equivalence between WLCs and EPs formation in PTSS as a tool for the realization of broadband MFFs. We consider PTSSs consisting of several (more than three) coupled cavities. In contrast to the two/three cavities and the periodic PTSSs cases, there are several configurations for realizing PTSSs consisting of multiple ($>3$) cavities, where each configuration exhibits different eigenvalues properties. We are interested in PTSSs comprising larger number of cavities as they can lead to the optimal design of higher-order MFFs exhibiting broader bandwidth and supporting higher communication rates. More specifically, we focus on PTSSs consisting of a chain of coupled passive cavities except for the first and last ones that exhibit, respectively, gain and loss of even magnitude, as seen in Fig. 2. We focus on this configuration because, as shown in Sec. II, it supports the formation of EPs of higher-order where *all* eigenvalues coalesce to a single point. This is in contrast to other PTSS configurations, which do not exhibit this property (see Sec. II and the Appendix). It should be noted that PTSSs consisting of infinite periodic arrays that have been studied previously have been designed to exhibit EPs of order 2. Moreover, the practical realization of such devices is more difficult and their functionality is limited by the propagation losses in the unit-cells [34]. Thus, the motivation for studying devices consisting of larger number of cavities (though not infinite) is clear as they provide enhanced performances while remaining practically realizable.

The rest of the paper is organized as follows: in Sec. II we discuss the general form of the PTSSs that are analyzed in this paper. We focus on the cases of PTSSs consisting of four and five cavities and derive the conditions at which all the eigenvalues of these systems coalesce, exhibiting fourth- and fifth-order EPs, respectively. In Sec. III we discuss the utilization these higher-order EPs for realizing broadband MFFs and in Sec. IV, we summarize the results and conclude. In the appendix we present the impact of incorporating more than a single gain and single loss cavities in the PTSS.

## II. MULTIRING STRUCTURES

In this section, we discuss the properties of an array of cavities with the general form depicted in Fig. 3. This structures consists of multiple coupled cavities of the same radius, where the first cavity includes a gain coefficient $g$ and the last cavity has a matching loss coefficient $-g$. All other cavities are assumed to be passive and lossless.

This case is particularly interesting as such structures can be straightforwardly used for filters design as further discussed below (see Sec. III). In order to satisfy the PTSS

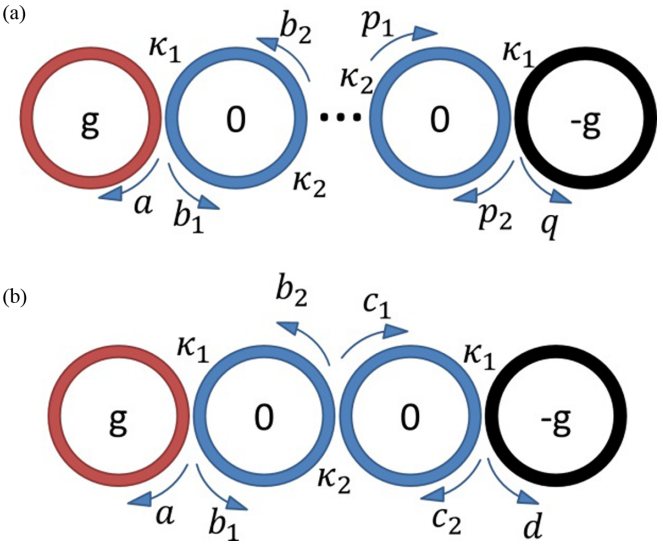


FIG. 3. (a) A general array of cavities, consisting of a single gain and a single matching loss. The field amplitudes of each zero-gain cavity can be fully described at the two points tangent to the neighbor cavities, and it depends on the coupling coefficients between the cavities. Note that for the construction of PTSSs, the coupling coefficients should be symmetric. (b) An example of such an array that contains four resonators. This configuration is further discussed in this paper.

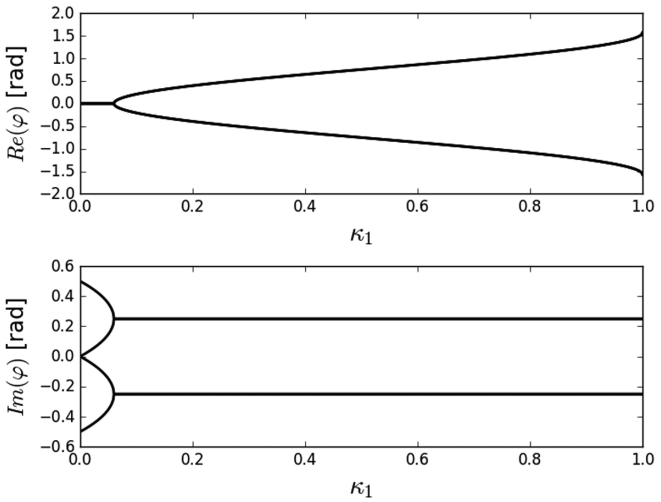


FIG. 4. Eigenvalue map for $g = 1$, $\kappa_2 = 0$. The upper panel depicts the real part of the eigenvalues while the lower panel shows the imaginary part. This map shows the phases that solve Eq. (3) for given parameters. In our case, $g$ and $\kappa_2$ are fixed and the map presents the phases that solve the equation for different $\kappa_1$ values. Similar maps can be plotted for other set of fixed and dynamic parameters.

conditions, all coupling coefficients should be symmetric. Let us consider the case of four coupled resonators, with two zero-gain cavities, depicted in Fig. 3(b). In this figure, the electric field amplitudes in each cavity are defined at the coupling points between adjacent microrings.

At steady-state, these amplitudes satisfy the following relations:

$$\begin{aligned}
a &= \sqrt{1-\kappa_1}e^{\frac{g}{2}}e^{i\varphi}a + i\sqrt{\kappa_1}e^{\frac{i\varphi}{2}}b_2,\\
b_1 &= i\sqrt{\kappa_1}e^{\frac{g}{2}}e^{i\varphi}a + \sqrt{1-\kappa_1}e^{\frac{i\varphi}{2}}b_2,\\
b_2 &= \sqrt{1-\kappa_2}e^{\frac{i\varphi}{2}}b_1 + i\sqrt{\kappa_2}e^{\frac{i\varphi}{2}}c_2,\\
c_1 &= i\sqrt{\kappa_2}e^{\frac{i\varphi}{2}}b_1 + \sqrt{1-\kappa_2}e^{\frac{i\varphi}{2}}c_2,\\
c_2 &= \sqrt{1-\kappa_1}e^{\frac{i\varphi}{2}}c_1 + i\sqrt{\kappa_1}e^{-\frac{g}{2}}e^{i\varphi}d,\\
d &= i\sqrt{\kappa_1}e^{\frac{i\varphi}{2}}c_1 + \sqrt{1-\kappa_1}e^{-\frac{g}{2}}e^{i\varphi}d,
\end{aligned} \tag{1}$$

where $\varphi$ is the round-trip phase, and $\kappa_i$ are the coupling coefficients defined in Fig. 3(b). This set of equations can be represented as a homogenous set and rewritten as $A \cdot \bar{v} = 0$ where $A$ is a $6 \times 6$ matrix and $\bar{v}$ is a vector of the field amplitudes. The eigenvalues of this matrix yield the resonant round-trip phases in the individual microresonators, corresponding to the resonance frequencies of the structure [35].

Requiring that the determinant of $A$ vanishes yields a characteristic equation of the following form:

$$0 = \sum_{k=0}^{N} c_k \cos(k\varphi), \tag{2}$$

where $N$ is the number of different coupling coefficients in the system. The parameters $c_k$ depend on the coupling coefficients between the resonators and on the gain coefficient $g$. The characteristic equation obtained for the discussed system is

$$\begin{aligned}
&2(\cos\varphi)^2 - 2\sqrt{1-\kappa_1}\left(\sqrt{1-\kappa_2} + \cosh\frac{g}{2}\right)\cos\varphi\\
&\quad - \kappa_1 + (2-\kappa_1)\sqrt{1-\kappa_2}\cosh\frac{g}{2} = 0.
\end{aligned} \tag{3}$$

Note that equation is quadratic in $\cos\varphi$. This is due to the fact that the system is symmetric and the given equation should be invariant under the transformation $\varphi \to -\varphi$. Consequently, the characteristic equation can be rewritten in the form:

The characteristic is indeed a second-order equation. Such an equation obtains two independent solutions for $\cos\varphi$ yielding overall four eigenvalues ($\varphi$ and $-\varphi$ are different solutions). The resulting round-trip phases are complex and depend on the specific parameters of the system. A useful technique of visualizing the unique characteristics of the system is to set $g$ and $\kappa_2$ and plot the real and imaginary part of the eigenvalues in the range $0 < \kappa_1 < 1$. Different $\kappa_2$ values have a different impact on the eigenvalues map.

The properties of PTSSs are derived from their eigenvalues; the solutions of their characteristic equation [e.g., Eq. (3) for the four-cavity case] or, in other words, the resonances of the PTSS. The real parts of the eigenvalues correspond to shifts in the resonance frequencies compared to an exponentially increase/decay of these solutions. The eigenvalues map (e.g., Fig. 4) provides a graphic description of the properties of the system solutions in its parameter space (i.e., the various coupling coefficients and gain/loss). Such maps allow for the identification of ranges in the parameters space where the solutions are, for example, purely real or complex. In particular, such maps reveal points at which the eigenvalues (or some of them) coalesce, thus forming EPs, and identify their order. Due to the large number of parameters

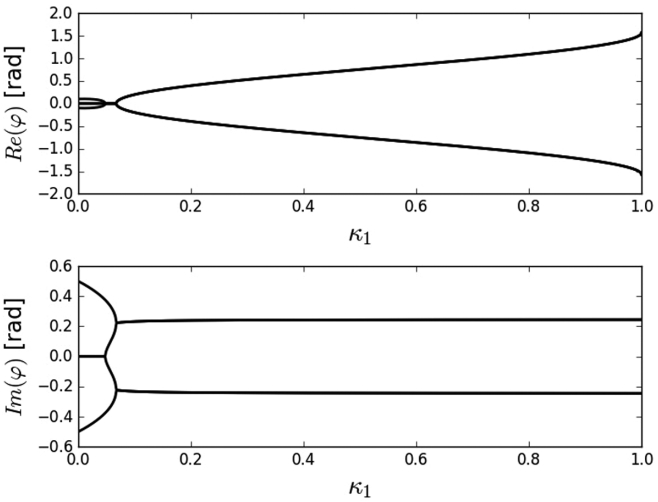


FIG. 5. Eigenvalue map for $g = 1, \kappa_2 = 0.01$. Note the formation of a small range in which all the solutions are purely imaginary, located between two EPs of order 2.

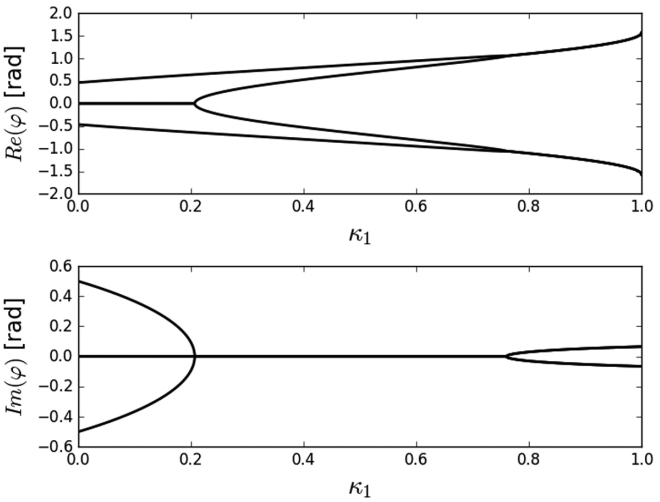


FIG. 6. Eigenvalue map for $g = 1$, $\kappa_2 = 0.2$. Here a large range at which the eigenvalues are purely real (similar to the completely passive case) is formed. As in Fig. 5, this range is located between two second-order EPs.

(two coupling coefficients and a gain/loss parameter in the case of four cavities) it is impossible to represent graphically the complete parameters' space (this is in contrast to the more commonly studied two- and three-cavity cases). Thus, the reasonable approach would be plotting partial eigenvalues maps where some of the parameters are fixed and the other are varied.

Returning to the eigenvalues of the four-cavity case, we first set the gain to be $g = 1$ and $\kappa_2 = 0$. This value of $\kappa_2$ implies that the system consists effectively of two isolated couples of cavities, each operating without interacting with the other. Note, that one of these pairs includes the gain section, while the other includes only the lossy section. The eigenvalues of this system are shown in Fig. 4. The two effectively separated systems possess a second-order EP at $\kappa_1 = 0.06$ and exhibit eigenvalues just as expected from an unbalanced structure: The system with the gain section exhibits eigenvalues that have positive imaginary parts. The other (lossy) system exhibits eigenvalues that have negative imaginary parts.

Increasing the coupling coefficient $\kappa_2$ yields a more interesting eigenvalues map as all four cavities can interact. For small $\kappa_2$ values (see Fig. 5 for $g = 1$, $\kappa_2 = 0.01$) the overall properties of the solutions remain rather similar although two EPs at different values of $\kappa_1$ are formed, at $\kappa_1 = 0.048$ and $\kappa_1 = 0.067$. It can be understood that these points originates from the $\kappa_1 = 0$ and $\kappa_1 = 0.06$ points for $\kappa_2 = 0$. As $\kappa_2$ is increased, the levels of $\kappa_1$ at which these EPs are formed shift to larger values.

Increasing the $\kappa_2$ value further changes the properties of the eigenvalues substantially. Figure 6 depicts the real and imaginary parts of the eigenvalues (as a function of $\kappa_1$) for $\kappa_2 = 0.2$. For high $\kappa_1$ values lower than $\sim 0.2$ two of the eigenvalues are purely real, while the other two are purely imaginary. Beyond that point, all eigenvalues become purely real, exhibiting four different resonant frequencies.

However, at relatively large $\kappa_1$ values ($\sim 0.75$) the eigenvalues coalesce into two pairs that exhibit both real and imaginary parts. This is because at very high coupling levels between the external resonator pairs, each pair effectively acts as a single cavity of twice the round-trip length.

At the extreme case of $\kappa_2 = 1$ the structure is effectively a system of three cavities where the roundtrip of the central (passive) resonator is twice that of the leftmost and rightmost cavities. The eigenvalues in this case are depicted in Fig. 7. A three cavity system exhibits three eigenvalues, where one of them is zero [22]. This is observed for $\kappa_1 < 0.632$ where two solutions are purely real and the other two are purely imaginary. However, at $\kappa_1 = 0.632$ a second-order EP is formed and the four solutions become purely real with four distinct resonance frequencies. It can be seen that on this scenario, all eigenvalues are either purely real or purely imaginary at any point.

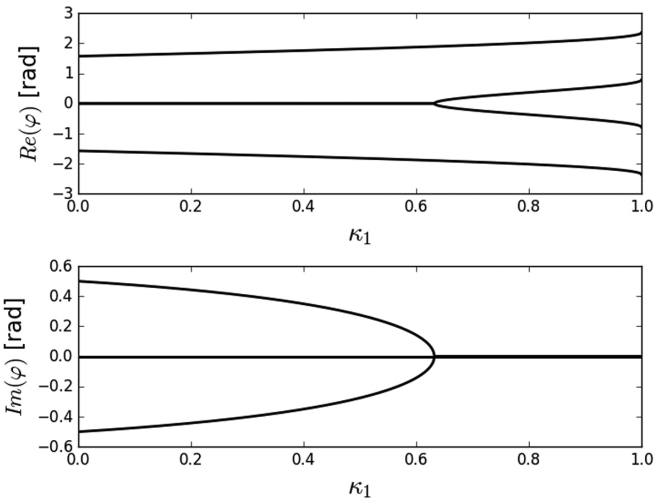


FIG. 7. Eigenvalue map for $g = 1$, $\kappa_2 = 1$. Note that in contrast to Fig. 6 there is no upper bound to the range at which purely real solutions are obtained.

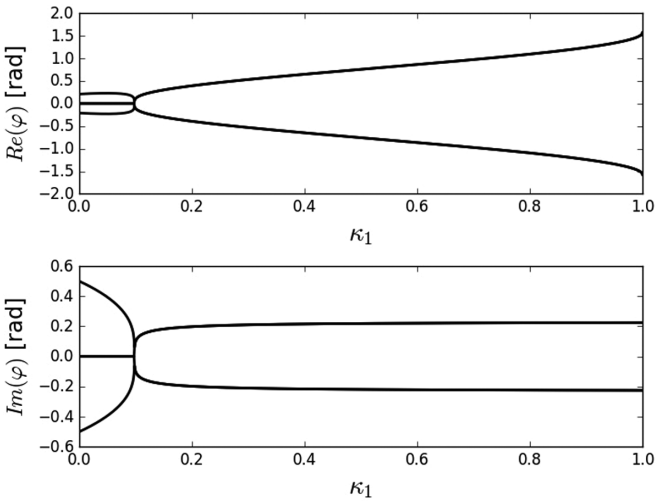


FIG. 8. Four-cavity systems' eigenvalues, where parameters are chosen such that fourth-order EP is formed. It can be seen that all phases coalesce at $\kappa_1 = 0.0979$. The rest of the coefficients are defined in the text.

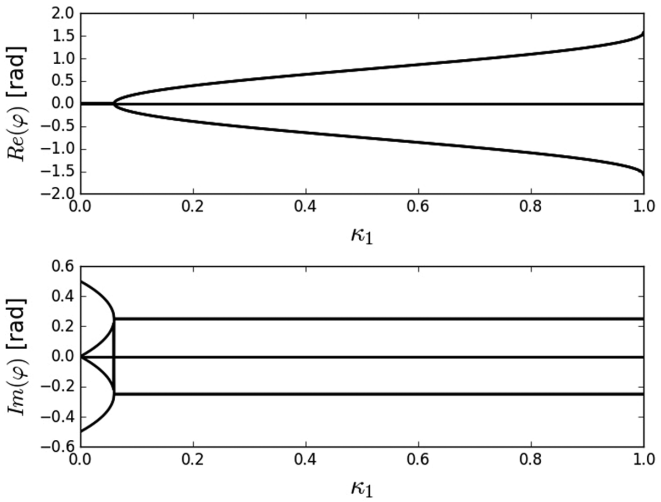


FIG. 9. Eigenvalue map for a five cavities PTSS, where $g = 1$ and $\kappa_2 = 0$. Two EPs of order 2 are formed at $\kappa_1 \approx 0.06$.

When $\kappa_2$ increased from zero to unity, the range in which all eigenvalues are purely real shrinks and then reexpands. Within this range there is a point at which this range becomes a point where *all* eigenvalues coalesce into a single value, thus forming a high-order EP. At this higher-order EP, all the eigenvalues are $\cos\varphi = 1$, or $\varphi = 0$. The coupling coefficients for which such scenario is obtained can be given by realizing that the characteristic equation should have the form of

$$C \cdot (1 - \cos\varphi)^{\lfloor \frac{N}{2} \rfloor} (\sin A\varphi)^{N \bmod 2} = 0, \tag{4}$$

where $N$ is the number of cavities in the system and $A$ is a rational number. It is not obvious that there is a valid set of coupling coefficients for which the characteristic Eq. (3) can indeed obtain the form of Eq. (4). This is because the coupling coefficients are limited to the range $0 < \kappa_i < 1$. In fact, as discussed further in the Appendix, fourth-order EPs are obtained only for *some* of the four-cavity PTSSs. Nevertheless, if such a set of coupling coefficients does exist, it can be found analytically comparing the coefficients of Eq. (3) to those of Eq. (4). In the discussed case of the four-cavity system ($N = 4$), the characteristic equation is quadratic and can be brought to the form (4) by selecting $C = 2$ and requiring that

$$\begin{aligned} -\kappa_1 + (2 - \kappa_1)\sqrt{1 - \kappa_2}\cosh\frac{g}{2} &= 2, \\ -2\sqrt{1 - \kappa_1}\left(\sqrt{1 - \kappa_2} + \cosh\frac{g}{2}\right) &= -4. \end{aligned} \tag{5}$$

Equations (5) yield the coupling coefficients for which a fourth-order EP is formed (for a given value of gain coefficient). For $g = 1$, the solution of Eq. (5) is easily found to be $\kappa_1 = 0.0979$, $\kappa_2 = 0.0432$. Figure 8 depicts the eigenvalues as a function of $\kappa_1$ for $\kappa_2 = 0.0432$. The point at which all four eigenvalues coalesce to a single solution, $\varphi = 0$, is clearly visible at $\kappa_1 = 0.0979$.

Having a PTSS exhibiting higher-order EP is highly attractive for many useful applications. Particularly, PTSSs operating at their EP has been shown to be highly useful for multiple applications including optical gyroscopes [36,37] and beam dynamics [38]. In addition, as discussed in Sec. III below, such PTSS are highly useful for constructing and optimizing broadband MFFs.

So far, we have discussed systems consisting of four cavities. Let us now examine the difference between this case and the case of five cavities. A PTSS consisting of five cavities has two different coupling coefficients: $\kappa_1$ between the leftmost and rightmost cavities to the internal adjacent cavities, and $\kappa_2$ between the middle cavity to its neighbors on both sides.

The steady state field amplitude equations can be written similarly to the case of four rings, and the homogenous set representation yields an $8 \times 8$ matrix. As for the four resonators case, by requiring the determinant of this matrix to vanish we obtain the following characteristic equation:

$$\begin{aligned} \Big[4\cos^2\varphi + 2\sqrt{1-\kappa_1}\Big(\sqrt{1-\kappa_2} + \kappa_2 - 2 - 2\sqrt{1-\kappa_1}\cosh\frac{g}{2}\Big) \\ \times \cos\varphi - 2(-2\sqrt{1-\kappa_2} + \kappa_1\sqrt{1-\kappa_2} + \kappa_2\sqrt{1-\kappa_1})\cosh\frac{g}{2} \\ + \kappa_1(\kappa_2 - 2)\Big] \cdot \sin\frac{\varphi}{2} = 0. \end{aligned} \tag{6}$$

Equation (6) consists of a product of a quadratic expression in $\cos\varphi$, and a sinusoidal term. The sinusoidal term yields a constant solution of $\varphi = 0$. It should be noted that such a solution is common to all PTSS comprising an odd number of elements [3]. The other four eigenvalues can be found by addressing only the quadratic part of the equation, by using the method described for the four-cavity case.

As for the four resonators case, we explore different eigenvalue maps obtained for different $\kappa_2$ values. Figure 9 depicts the map for $\kappa_2 = 0$.

At this condition, this system consists of effectively three separated structures, two comprising two cavities and an isolated resonator. This is quite similar to the case depicted in Fig. 4 with the addition of the isolated cavity exhibiting the $\varphi = 0$ solution. As could be expected, the solutions are rather similar to the four-ring case; however, there is a constant solution given from the sinusoidal term in Eq. (6). The separated

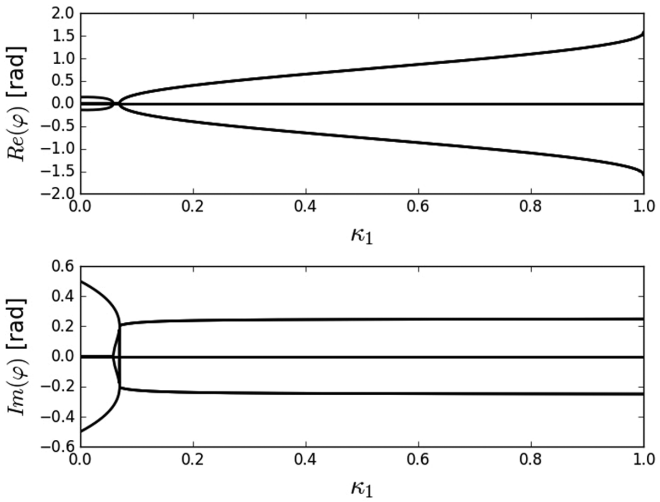


FIG. 10. Eigenvalue map for five cavities, where $g = 1$ and $\kappa_2 = 0.01$. Note the formation of a range at which the solutions are purely imaginary as in Fig. 5 for the four-cavity structure

systems have a second-order EP at $\kappa_1 = 0.06$, just as in the four-cavity case.

Figure 10 depicts an eigenvalue map for $\kappa_2 = 0.01$. It can be seen that two EPs are formed, at $\kappa_1 = 0.059$ and $\kappa_1 = 0.069$. It is interesting to compare these values to the EP locations of the four-cavity case for this case ($\kappa_2 = 0.01$) as seen in Fig. 5. Although the overall dynamics are similar, the shift in the positions of the two EPs with respect to changes in $\kappa_2$ is somewhat larger. This introduces a characteristic of multicavity systems that will be further discussed in Sec. III; the more cavities the system includes, the more sensitive it is to parameter changes.

Further increasing $\kappa_2$ yields a similar eigenvalues map, as can be seen in Fig. 11, depicting the case of $\kappa_2 = 0.2$. As for lower $\kappa_2$ values, one eigenvalue is consistently zero, while the others are divided into two pairs, each consisting of two merged eigenvalues.

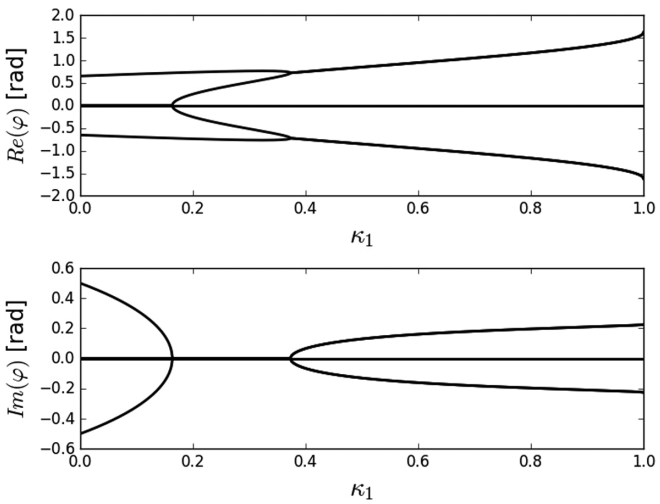


FIG. 11. Eigenvalue map for five cavities, where $g = 1$ and $\kappa_2 = 0.2$. As in the four-cavity case (Fig. 6) increasing $\kappa_2$ yields a range at which all eigenvalues are purely real.

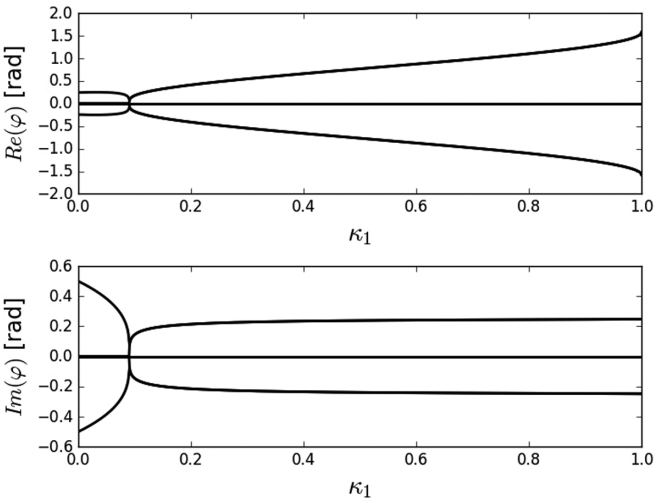


FIG. 12. Eigenvalue map for five cavities, where $g = 1$ and $\kappa_2 = 0.0296$, forming a fifth-order EP.

Except for the constant zero solution, this image is much more similar to the one depicted in Fig. 6. It can be seen that for small values of $\kappa_1$ two of the eigenvalues are purely real while the other pair is purely imaginary. The second-order EP at which the eigenvalues become all real is located at $\kappa_1 = 0.16$. Beyond that point, there is a range of $\kappa_1$ values for which all eigenvalues are real, up to $\kappa_1 = 0.37$. The range at which all four eigenvalues are real varies with respect to $\kappa_2$. Similar to the four rings case discussed previously, there is a value of $\kappa_2$ at which all five eigenvalues coalesce to a single point, forming a fifth-order EP. This point can be found by requiring that the cosine part of Eq. (6) has the form of Eq. (4).

A similar approach can be applied to structures incorporating more cavities, which can yield higher-order EPs. For $N = 5$, it is clear that the sinusoidal term obtains the constant zero solution. The remaining part of the characteristic equation is quadratic in $\cos\varphi$ where for all solutions to coalesce at $\varphi = 0$ it is required that

$$2\sqrt{1-\kappa_1}\left(\sqrt{1-\kappa_2}+\kappa_2-2-2\sqrt{1-\kappa_1}\cosh\frac{g}{2}\right)=-8,$$
$$-2(-2\sqrt{1-\kappa_2}+\kappa_1\sqrt{1-\kappa_2}+\kappa_2\sqrt{1-\kappa_1})\cosh\frac{g}{2}$$
$$+\kappa_1(\kappa_2-2)=4. \tag{7}$$

For $g = 1$, the solution of this set is easily found to be $\kappa_1 = 0.0905$, $\kappa_2 = 0.0296$. Figure 12 plots the eigenvalues of the five-ring structure as a function of $\kappa_1$ for $\kappa_2 = 0.0296$ and $g = 1$. The formation of a fifth-order EP at $\kappa_1 \approx 0.1$ is clearly seen.

## III. MAXIMALLY FLAT FILTERS

As discussed in the introduction, a system operating at its EP forms a WLC and therefore resonates over a wide range of frequencies [28]. Consequently, the parameters at which EPs (and especially high-order EPs) are obtained can be used for designing MFFs. The underlying idea for the construction of this MFF is that at the higher-order EP of a PTSS (e.g., a fifth-order EP of a five-cavity PTSS), the conventional round-trip phase in the active cavity (the one with the gain) is

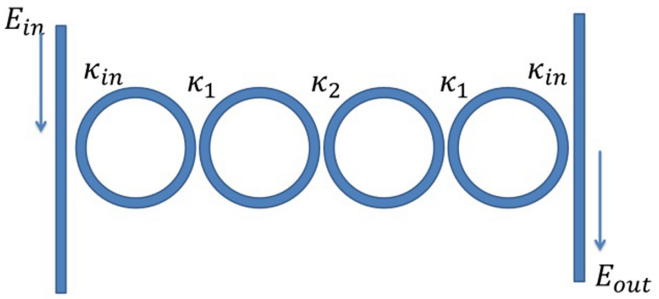


FIG. 13. A MFF constructed of four passive lossless cavities. For maximal flatness, coupling coefficients between the rings should be chosen according to the EP conditions of the four-cavity systems.

compensated by the phase response of the other cavities, thus yielding a WLC. Note, that by finding this high-order EP we obtain the coupling coefficients between the microresonators, $\kappa_i$, which are required in order to turn the leftmost resonator (see, e.g., Fig. 3) into a WLC. The rightmost, lossy cavity can be effectively replaced by a transparent one, which is coupled to an I/O waveguide with the coupling coefficient $\kappa_{\text{in}}$:

$$\sqrt{1-\kappa_{\text{in}}} = e^{-\frac{g}{2}}. \tag{8}$$

This value is chosen to have the same impact as loss $-g$ in the last cavity.

Finally, the gain material in the leftmost cavity in Fig. 3, which includes gain in the PTSS configuration, is replaced by a passive one that is coupled to an I/O waveguide with the coupling coefficient $\kappa_{\text{in}}$ defined in Eq. (8), as depicted in Fig. 13. This is in order to form an overall critically coupled WLC and obtain maximal transmission at the drop port of the filter. The resulting filter is an MFF as it resonates, effectively, over a broadband and is critically coupled.

To demonstrate this idea we consider filters consisting of three, four, and five cavities and examine their spectral response with respect to the gain $g$ (or equivalently the $\kappa_{\text{in}}$). As a concrete example we assume that the cavities are realized using SOI platform (effective index of $\sim$3.0) with a radius of 10 $\mu$m. According to these parameters, the relation between the round-trip phase and the spectral detuning from resonance is

$$\Delta\nu = \phi \cdot \frac{c}{2\pi n_g L} = \phi \cdot \frac{c}{4\pi^2 n_g R}, \tag{9}$$

where $n_g$ is the group index and $L$ is the round-trip length.

Figure 14 depicts the spectral transmission function $|E_{\text{out}}/E_{\text{in}}|^2$ of various filters designed using the above-mentioned approach. The coupling coefficients used are detailed in Table I. The flatter transmission band and the broader bandwidth of higher-order filters are clearly evident, as well

TABLE I. Coupling coefficients that produce the plot of Fig. 14.

| Structure | Coupling Coefficients |
|---|---|
| Three cavities | $\kappa_{\text{in}} = 0.6321,\ \kappa_1 = \kappa_2 = 0.118$ |
| Four cavities | $\kappa_{\text{in}} = 0.6321,\ \kappa_1 = \kappa_3 = 0.0979,\ \kappa_2 = 0.0432$ |
| Five cavities | $\kappa_{\text{in}} = 0.6321,\ \kappa_1 = \kappa_4 = 0.0905,\ \kappa_2 = \kappa_3 = 0.0296$ |

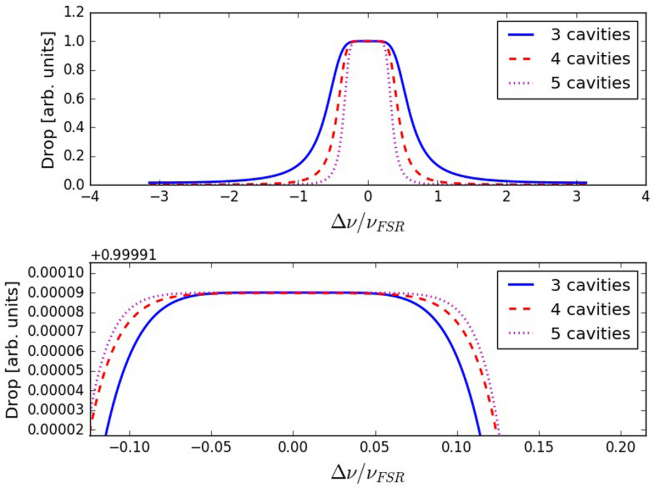


FIG. 14. Upper figure depicts the drop functions of filters comprised of three, four, and five cavities, where each case the coupling coefficients has been chosen according to those that bring the corresponding PTSS to its highest-order EP. Lower figure depicts zoom-in on the resonance frequencies. It can be clearly seen that the transmission is indeed flat and that the five-cavity structure achieves the widest response, as expected. In this illustration, the cavities are assumed to be silicon-on-insulator (SOI), with effective index of $\sim$3.0 and radius of 10 $\mu$m.

as the steeper fall of the transmission outside the transmission band (corresponding to a "boxlike" shape), which render these filters closer to an ideal filter.

For comparison, Fig. 15 depicts the transmission function of a four-cavity MFF with $\kappa_{\text{in}} = 0.259181$ designed according

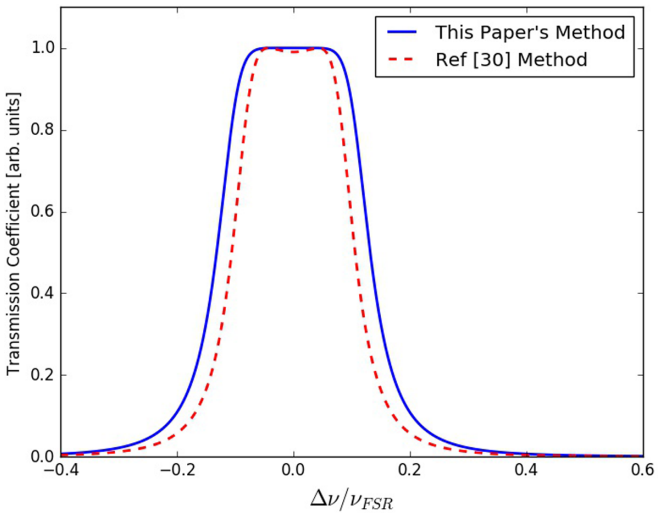


FIG. 15. Comparison between the transmission function of filters designed according to the method described here (blue, solid) to that of Ref. [30] (red, dashed). The coupling coefficients yielded by our approach are: $\boldsymbol{\kappa_{\text{in}}} = 0.259181$, $\boldsymbol{\kappa_1} = 0.00927232$, $\boldsymbol{\kappa_2} = 0.00386386$ while those yielded by the method of Ref. [30] are: $\boldsymbol{\kappa_{\text{in}}} = 0.259181$, $\boldsymbol{\kappa_1} = 0.00671751$, $\boldsymbol{\kappa_2} = 0.00268701$. The advantage of our approach is clear, especially for larger coupling coefficients, where the common methods yields a rippled filter response. We note that our approach is still advantageous even in weak coupling regime, as it provides a wider transmission bandwidth.

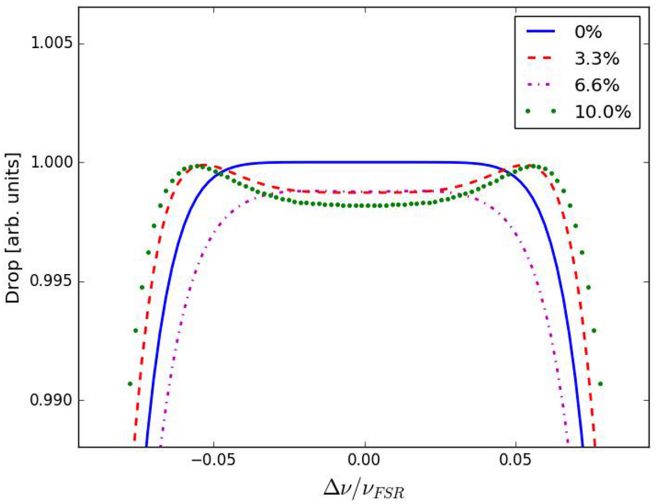


FIG. 16. Impact of coupling noise level on the filter responses. Each plot corresponds to a different level of Gaussian noise that is added to every coupling coefficient of the filter designed in Fig. 15. The variance of the added noise is a given percentage of the coupling coefficient itself. Due to the statistical properties of the noise, this example is just one of many other options.

to the PTSS approach, to a similar MFF designed according to the commonly used approach described in Ref. [30]. As seen in Fig. 15, the PTSS design approach yields wider transmission bandwidth and enhance the width of the flat band. As some of the coupling coefficients in this example are relatively large, the approach of Ref. [30] (which assumes small coupling) yield a nonflat filer exhibiting substantial ripple. In contrast, the design approach described here yields a flat response where the width of the flat band (defined by the width above 0.9 transmission) is larger by 11.17%.

The design procedure presented here yields specific physical parameters (e.g., coupling coefficients) leading to maximally flat filters (as seen in Fig. 15). However, any practical fabrication process introduces, necessarily, errors and disorder in the actual coupling coefficients and resonances [39,40]. While resonance shifts can be tuned and corrected using a variety of methods (thermo-optical effects, UV post-tuning, etc.), modifying the coupling coefficients is less trivial. Therefore, in the context of this paper, it is important to study the impact of a coupling noise on the resulting filter response.

We consider a four-cavity system that includes three different coupling coefficients $\kappa_{\text{in}}$, $\kappa_1$, and $\kappa_2$. The impact of fabrication errors is introduced as an additive Gaussian noise $\sim N(0, \sigma_{\text{d}})$ applied to each coupling coefficient separately. Note that the noise not only affects the relation between $\kappa_1$ and $\kappa_2$, but also breaks the symmetry properties of the structure. The applied variations in the coupling coefficients are proportional to the nominal coupling value (i.e., larger coupling coefficients experience larger nominal variations). Figure 16 depicts the modification of the filter frequency response due to noise with different variance levels. As the noise level increases, the bandwidth decreases and ripples evolve across the passband. Nevertheless, the ripples are on the order of $\sim$1% of the transmission, which is still substantially smaller than the maximal allowed ripple level for telecommunication applications ($\sim$11%).

## IV. CONCLUSION

We have studied the properties of PTSSs comprising multiple (4–5) cavities. For some of the possible PTSS configurations, proper choice of parameters can lead to the formation of high-order EPs. The set of parameters leading to such points can be obtained by requiring that all eigenvalues coalesce, leading to a simple set of algebraic equations. At such a high-order EP, the system resonates over a wide and continuous range of frequencies, thus forming a white-light cavity. The equivalence between the high-order EP and WLC facilitates the design of optical MFFs consisting of coupled optical cavities.

The order of the EP is determined by the number of the coupled cavities. Using the method described here, any order of EP can be constructed by solving the characteristic equation of the system, and yield the corresponding MFF. The EP-based design method enhances the filter performances, yielding a broader and flatter spectral response compared to the commonly used approaches [30].

It should be noted that unlike methods which are based on coupled cavities rate equation analysis, the design approach presented here is also valid for large coupling coefficients. This is important because the weak coupling approximation (which is inherent to rate equations analysis) induces limitations on the ability to describe accurately systems comprising large number of cavities. Such a system necessitates relatively large coupling coefficients towards the edges of the coupled cavity array, thus rendering the rate equations model less accurate. The connection between filter design theory and physical understanding of coupled optical cavities systems discussed here, facilitates the development of various applications such as optical sensors, superluminal lasers, optical buffers, and many more.

## ACKNOWLEDGMENT

The authors are grateful to S. Shahriar for useful discussions and insightful comments.

## APPENDIX: GENERALIZED FOUR-CAVITY PTSS

This appendix introduces various configurations of PTSSs consisting of coupled resonators, showing that higher-order EPs cannot be obtained in all of them. Although we focus on arrays comprising four coupled cavities, we believe that some of the conclusions can be generalized for larger arrays. Requiring that the four-cavity system is parity time (PT)-symmetric, there are four possibilities of arrangements, as seen in Fig. 17.

Here, red cavities (marked "g") include gain, black cavities (marked "-g") are lossy and blue cavities (marked "0") are considered as transparent. We note that the configurations in Fig. 17(c) and Fig. 17(d) can be further generalized by considering different gain levels in the red cavities (and corresponding losses in the black ones), as will be further shown.

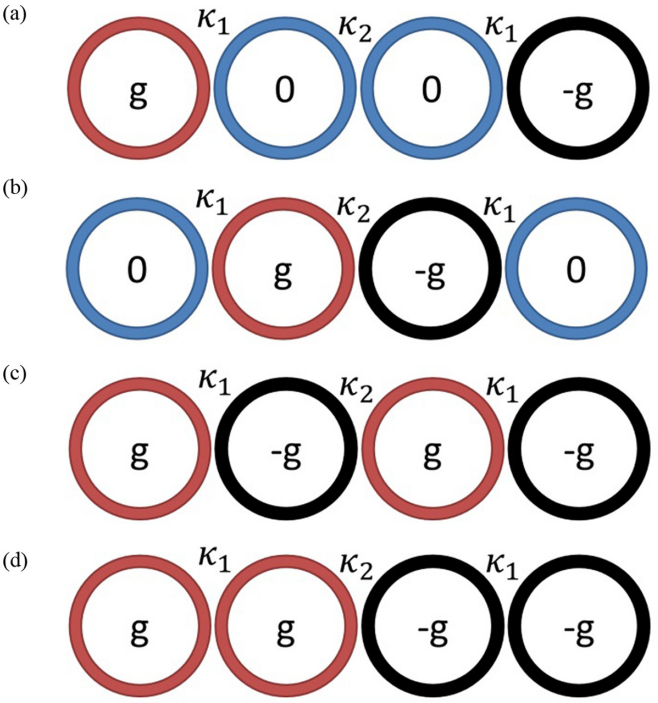


FIG. 17. All possible structures of four coupled cavities, assuming all active cavities are of the same gain.

The structure In Fig. 17(a) corresponds to the one discussed in the main text of the paper. This structure has been shown to support a fourth-order EP (see Fig. 3). For completeness, let us now consider the other structures. Using a similar method as that used for obtaining Eq. (3), the characteristic equation corresponding to the eigenvalues of structure 17(b) can be found to be

$$2(\cos\varphi)^2 - 2\sqrt{1-\kappa_1}\left(1+\sqrt{1-\kappa_2}\cosh\frac{g}{2}\right)\cos\varphi$$
$$-\kappa_1 + (2-\kappa_1)\sqrt{1-\kappa_2}\cosh\frac{g}{2} = 0. \quad \text{(A1)}$$

In order to find whether configuration 17 (b) supports a fourth-order EP, we follow the approach outlined in Sec. II. Requiring that all eigenvalues coalesce at $\varphi = 0$, it can be easily shown that for any value of $g$, this requirement is obtained only for $\kappa_1 = 0$ (In the specific case of $g = 1$ the coupling coefficients are $\kappa_1 = 0$, $\kappa_2 = 0.213$). This is a degenerate configuration that separates the array into three distinct subsystems: a PTSS comprising two cavities and two individual transparent cavities. Thus, even though all the eigenvalues correspond to $\varphi = 0$, this does not result in a fourth-order EP. We can conclude that configuration 17(b) does not support a higher-order EP.

In a similar way, the characteristic equation of structure 17(c) is

$$2(\cos\varphi)^2 - 2\sqrt{1-\kappa_1}(1+\sqrt{1-\kappa_2})\cosh\frac{g}{2}\cos\varphi - \kappa_1$$
$$+(1+(1-\kappa_1)\cosh g)\sqrt{1-\kappa_2} = 0. \quad \text{(A2)}$$

Again, by requiring that all eigenvalues coalesce at $\varphi = 0$, it can be mathematically shown that the solution is $\kappa_2 = 0$, for every value of $g$. For $g = 1$ the results for the coupling coefficients are $\kappa_1 = 0.213$, $\kappa_2 = 0$. As was claimed for structure 17(b), this is also a degenerate case where the structure is separated into two PTSSs comprising two cavities each. Note that structures 17(b) and 17(c) can be separated into PT-symmetric subsystems (a passive cavity is also a PTSS) by setting $\kappa_1$ and $\kappa_2$ to zero, respectively. Therefore, these structures can satisfy the condition of all round-trip phase eigenvalues equal to zero without forming a fourth-order EP. On the other hand, structures 17(a) and 17(d) cannot be separated into PT-symmetric subsystems and can, therefore, potentially exhibit fourth-order EP.

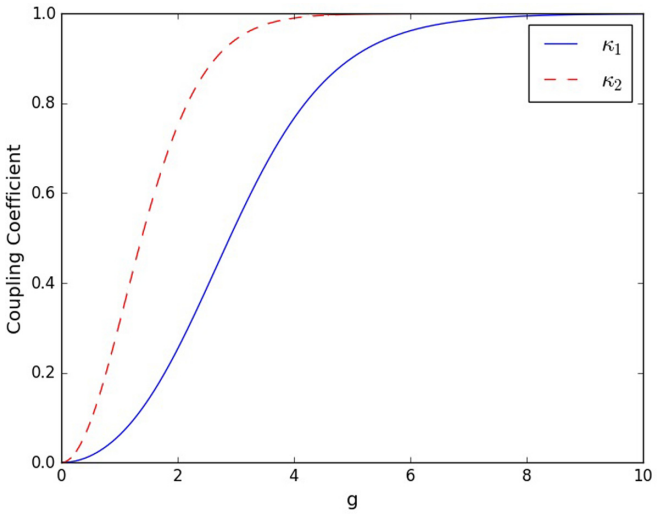


FIG. 18. Required coupling coefficients for a higher-order EP to form in structure (d). It can be seen that $\kappa_2 > \kappa_1$ and that a solution exists for every value of $g$.

By applying the exact same method to structure 17(d), the characteristic equation is given by

$$2\cos^2\varphi - 2\sqrt{1-\kappa_1}(1+\sqrt{1-\kappa_2})\cosh\frac{g}{2}\cos\varphi - 1$$
$$+(1-\kappa_1)(1+\sqrt{1-\kappa_2}) + \sqrt{1-\kappa_2}\cosh g = 0. \quad \text{(A3)}$$

The solution of this equation depends on $g$, and might support a fourth-order EP at which none of the coupling coefficients vanish. Consider, for example, the case of $g = 1$, with the coupling parameters $\kappa_1 = 0.061$ and $\kappa_2 = 0.310$. For these values, a fourth-order EP is formed in the system. Figure 18 plots the coupling coefficients needed for obtaining a fourth-order EP in the system as a function of the gain parameter. Interestingly, obtaining a fourth-order EP requires that $\kappa_2 > \kappa_1$ for every gain level. This is in contrast to the

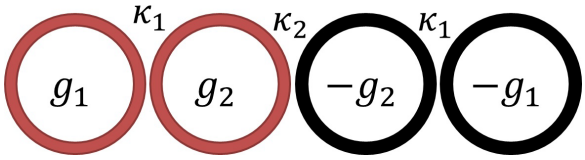


FIG. 19. A generalized four-cavity structure that satisfies the PTSS conditions. Both $g_1$ and $g_2$ can be either positive or negative. Any of the structures presented in Fig. 17 can be given by a selection of $g_1$ and $g_2$ here.

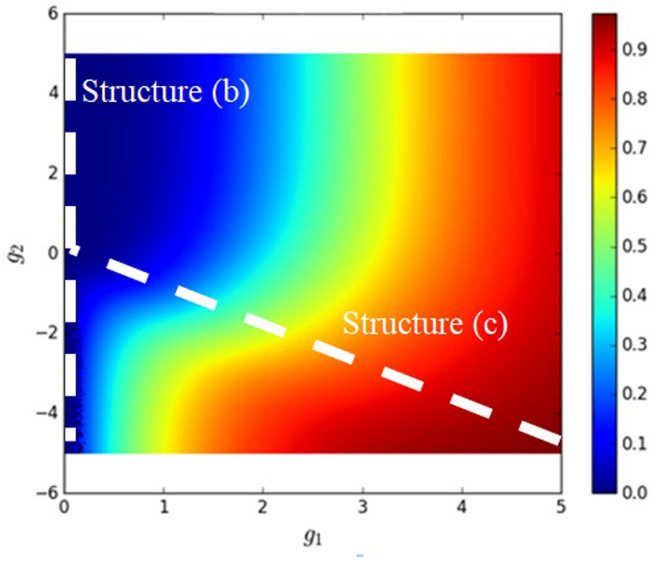


FIG. 20. $\kappa_1$ values that solve Eq. (A4), with respect to $\boldsymbol{g}_1$ and $\boldsymbol{g}_2$.

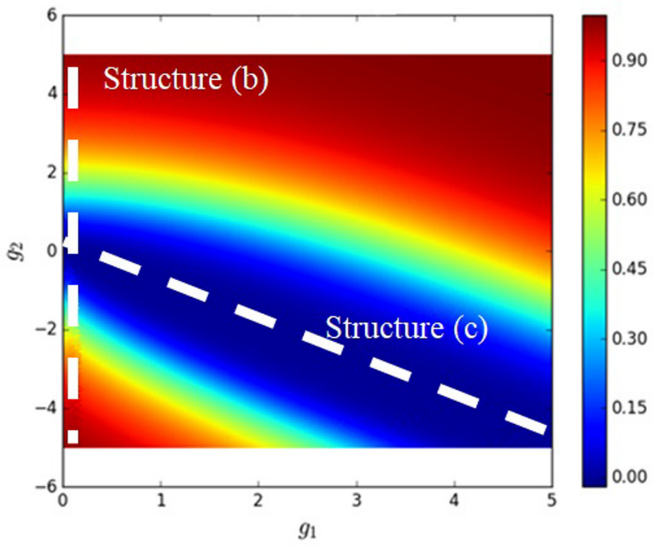


FIG. 21. $\kappa_2$ values that solve Eq. (A4), with respect to $\boldsymbol{g}_1$ and $\boldsymbol{g}_2$.

requirement for structure 17(a), for which the requirement is inverse.

Structure 17(d) can be further generalized by removing the constraint of identical gain parameters in the system. Without this constraint, all of the structures in Fig. 17 coalesce into a single structure, as seen in Fig. 19.

The characteristic equation of the generalized case is

$$-2(\cos\varphi)^2 + 2\sqrt{1-\kappa_1}\left(\cosh\frac{g_1}{2} + \sqrt{1-\kappa_2}\cosh\frac{g_2}{2}\right)\cos\varphi + \kappa_1 - (2-\kappa_1)\sqrt{1-\kappa_2}\cosh\frac{g_1}{2}\cosh\frac{g_2}{2} - \kappa_1\sqrt{1-\kappa_2}\sinh\frac{g_1}{2}\sinh\frac{g_2}{2} = 0. \quad \text{(A4)}$$

For simplicity, let us assume that $g_1 > 0$. Under this condition, a generalized version of structure 17(c) and structure 17(d) can be obtained by taking $g_2 < 0$ and $g_2 > 0$, respectively. Figures 20 and 21 depict the values of $\kappa_1$ and $\kappa_2$ required for the formation of a higher-order EP over the range $0 < g_1 < 5$ and $-5 < g_2 < 5$, respectively.

Note that for every choice of $g_1$ and $g_2$ there is a set of coupling coefficients for which all the eigenvalues are zero. The dashed white lines correspond to the degenerate cases $g_1 = 0$ [structure 17(b)] and $g_1 = -g_2$ [structure 17(c)]. On these lines the solution does not correspond to a fourth-order EP but rather to the separation of the four-cavity array into several distinct subystems. This is manifested by the fact that on these lines either $\kappa_1$ or $\kappa_2$ vanish as discussed above.


[1] M. A. Miri and A. Alu, Exceptional points in optics and photonics, Science **363**, eaar7709 (2019).

[2] Z.-P Liu, J. Zhang, S. K. Ozdemir, B. Peng, H. Jing, X.-Y. Lu, C.-W. Li, L. Yang, F. Nori, and Y.-X. Liu, Metrology with Pt-Symmetric Cavities: Enhanced Sensitivity Near the PT-Phase Transition, Phys. Rev. Lett. **117**, 110802 (2016).

[3] H. Hodaei, A. U. Hassan, S. Wittek, H. G. Garcia, R. El-Ganainy, D. N. Christodoulides, and M. Khajavikhan, Enhanced sensitivity at higher-order exceptional points, Nature (London) **548**, 187 (2017).

[4] A. Lupu, H. Benisty, and A. Degiron, Using optical PT-Symmetry for switching applications, Photonic. Nanostruct. **12**, 305 (2014).

[5] H. Jing, S. K. Ozdemir, X. Y. Lu, J. Zhang, L. Yang, and F. Nori, PT-symmetric phonon laser, Phys. Rev. Lett. **113**, 053604 (2014).

[6] J. M. Lee, S. Factor, Z. Lin, I. Vitebskiy, F. M. Ellis, and T. Kottos, Reconfigurable Directional Lasing Modes in Cavities with Generalized PT Symmetry, Phys. Rev. Lett. **112**, 253902 (2014).

[7] M. Veysi, M. A. K. Othman, A. Figotin, and F. Capolino, Degenerate band edge laser, Phys. Rev. B **97**, 195107 (2018).

[8] M. Y. Nada, M. A. K. Othman, and F. Capolino, Theory of coupled resonator optical waveguides exhibiting high-order exceptional points of degeneracy, Phys. Rev. B **96**, 184304 (2017).

[9] Z. Lin, H. Ramenzani, T. Eichelkraut, T. Kottos, H. Cao, and D. N. Christodoulides, Unidirectional Invisibility Induced by Pt-Symmetric Periodic Structures, Phys. Rev. Lett. **106**, 213901 (2011).

[10] M. A. K. Othman, X. Pan, G. Atmatzakis, C. G. Christodoulou, and F. Capolino, Experimental demonstration of degenerate band edge in metallic periodically loaded circular waveguide, IEEE Trans. Microwave Theory Tech. **65**, 4037 (2017).

[11] H. Hodaei, M. A. Miri, A. U. Hassan, W. E. Hayenga, M. Heinrich, D. N. Christodoulides, and M. Khajavikhan, Parity-time-symmetric coupled microring lasers operaeting aroung an exceptional point, Opt. Lett. **40**, 4955 (2015).

[12] L. Chang, X. Jiang, S. Hua, C. Yang, J. Wen, L. Jiang, G. Li, G. Wang, and M. Xiao, Parity-time symmetry and variable op-

tical isolation in active-passive-coupled microresonators, Nat. Photonics **8**, 524 (2014).
[13] H. Hodaei, M. A. Miri, M. Heinrich, D. N. Christodoulides, and M. Khajavikhan, Parity-time-symmetric microring lasers, Science **346**, 975 (2014).
[14] L. Feng, R. El-Ganainy, and L. Ge, Non-hermitian photonics based on parity-time symmetry, Nat. Photonics **11**, 752 (2017).
[15] B. Peng, S. K. Ozdemir, F. Lei, F. Monifi, M. Gianfreda, G. L. Long, S. Fan, F. Nori, C. M. Bender, and L. Yang, Parity-time-symmetric whispering-gallery microcavities, Nat. Phys. **10**, 394 (2014).
[16] L. Feng, Z. J. Wong, R. Ma, Y. Wang, and X. Zhang, Single-mode laser by parity-time symmetry breaking, Science **346**, 972 (2014).
[17] J. Schnabel, H. Cartarius, J. Main, G. Wunner, and W. D. Heiss, PT-symmetric waveguide system with evidence of a third-order exceptional point, Phys. Rev. A **95**, 053868 (2017).
[18] K. Ding, G. Ma, M. Xiao, Z. Q. Zhang, and C. T. Chan, Emergence, Coalescence, and Topological Properties of Multiple Exceptional Points and Their Experimental Realization, Phys. Rev. X **6**, 021007 (2016).
[19] R. El-Ganainy, M. Khajavikhan, and L. Ge, Exceptional points and lasing self-termination in photonic molecules, Phys. Rev. A **90**, 013802 (2014).
[20] X. Zhou, S. K. Gupta, Z. Huang, Z. Yan, P. Zhan, Z. Chen, M. Lu, and Z. Wang, Optical lattices with higher-order exceptional points by non-Hermitian coupling, Appl. Phys. Lett. **113**, 101108 (2018).
[21] M. Y. Nada, M. A. K. Othman, O. Boyraz, and F. Capolino, Giant resonance and anomalous quality factor scaling in degenerate band edge coupled resonator optical waveguides, J. Lightwave Technol. **36**, 3030 (2018).
[22] J. Scheuer and M. S. Shahriar, Trap-door optical buffering using a flat-top coupled microring filter: The superluminal cavity approach, Opt. Lett. **38**, 3534 (2013).
[23] A. Wicht, K. Danzmann, M. Fleischhauer, M. Scully, G. Müller, and R. H. Rinkleff, White-light cavities, atomic phase coherence, and gravitational wave detectors, Opt. Commun. **134**, 431 (1996).
[24] H. N. Yum, Y. J. Jang, X. Liu, and M. S. Shahriar, Visualization of superluminal pulses inside a white light cavity using plane wave spatio temporal transfer functions, Opt. Express **20**, 18898 (2012).
[25] D. D. Smith, K. Myneni, J. A. Odutola, and J. C. Diels, Enhanced sensitivity of a passive optical cavity by an intracavity dispersive medium, Phys. Rev. A **80**, 011809(R) (2009).
[26] D. D. Smith, H. Chang, L. Arissian, and J. C. Diels, Dispersion-enhanced laser gyroscope, Phys. Rev. A **78**053824 (2008).
[27] G. S. Pati, M. Salit, K. Salit, and M. S. Shahriar, Demonstration of a Tunable-Bandwidth White-Light Interferometer Using Anomalous Dispersion in Atomic Vapor, Phys. Rev. Lett. **99**, 133601 (2007).
[28] J. Scheuer, White light cavity formation and superluminal lasing near exceptional points, Opt. Express **26**, 32091 (2018).
[29] O. Kotlicki, J. Scheuer, and M. S. Shahriar, Theoretical study on Brillouin fiber laser sensor based on white light cavity, Opt. Express **20**, 28234 (2012).
[30] B. E. Little, S. T. Chu, H. A. Haus, J. Foresi, and J.-P. Laine, Microring resonator channel dropping filters, J. Lightwave Technol. **15**, 998 (1997).
[31] B. E. Little, S. T. Chu, P. P. Absil, J. V. Hryniewicz, F. G. Johnson, F. Seiferth, D. Gill, V. Van, O. King, and M. Trakalo, Very high-order microring resonator filters for wdm applications, IEEE Photonics Technol. Lett. **16**, 2263 (2004).
[32] B. E. Little, S. T. Chu, J. V. Hryniewicz, and P. P. Absil, Filter synthesis for periodically coupled microring resonators, Opt. Lett. **25**, 344 (2000).
[33] C. K. Madsen and J. H. Zhao, *Optical Filter Design and Analysis: A Signal Processing Approach* (Wiley-Interscience, New York, 1999).
[34] J. K. S. Poon, J. Scheuer, Y. Xu, and A. Yariv, Designing coupled-resonator optical waveguide delay lines, J. Opt. Soc. Am. B **21**, 1665 (2004).
[35] M. Y. Nada, T. Mealy, F. Yazdi, A. F. Abdelshafy, A. Figotin, and F. Capolino, General Conditions to Realize Exceptional Points of Degeneracy and Applications, in *12th International Congress on Artificial Materials for Novel Wave Phenomena* (IEEE, Espoo, Finland, 2018).
[36] J. Ren, H. Hodaei, G. Harari, A. U. Hassan, W. Chow, M. Soltani, D. Christodoulides, and M. Khajavikhan, Ultrasensitive microscale parity-time-symmetric ring laser gyroscope, Opt. Lett. **42**, 1556 (2017).
[37] D. D. Smith, H. Chang, L. Horstman, and J. C. Diels, Parity-time-symmetry-breaking gyroscopes: Lasing without gain and subthreshold regimes, Opt. Express **27**, 34169 (2019).
[38] M. C. Zheng, D. Christodoulides, R. Fleischmann, and T. Kottos, PT optical lattives and universality in beam dynamics, Phys. Rev. A **82**, 010103(R) (2010).
[39] S. Mookherjea and A. Oh, Effect of disorder on slow light velocity in optical slow-wave structures, Opt. Lett. **32**, 289 (2007).
[40] F. Florio, D. Kalantarov, and C. P. Search, Effect of static disorder on sensitivity of coupled resonator optical waveguide gyroscopes, J. Lightwave Technol. **32**, 4020 (2014).